Neurotherapeutics 21 (2024) e00439

Contents lists available at ScienceDirect

Neurotherapeutics

journal homepage: www.sciencedirect.com/journal/neurotherapeutics

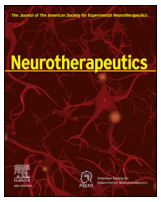

Original Article

A combination of Δ^9-tetrahydrocannabinol and cannabidiol modulates glutamate dynamics in the hippocampus of an animal model of Alzheimer's disease

Nuria Sánchez-Fernández [a,b], Laura Gómez-Acero [a,b], Anna Castañé [c,d,e,f], Albert Adell [e,g], Leticia Campa [c,e,h], Jordi Bonaventura [a,b], Verónica Brito [d,h,i], Silvia Ginés [d,h,i], Francisco Queiróz [j], Henrique Silva [j], João Pedro Lopes [j], Cátia R. Lopes [j], Marija Radošević [d,h], Xavier Gasull [d,h], Rodrigo A. Cunha [j,k], Attila Köfalvi [l], Samira G. Ferreira [j], Francisco Ciruela [a,b], Ester Aso [a,b,*]

[a] *Pharmacology Unit, Department of Pathology and Experimental Therapeutics, School of Medicine and Health Sciences, Institute of Neurosciences, University of Barcelona, 08907 L'Hospitalet de Llobregat, Spain*
[b] *Neuropharmacology and Pain Group, Neuroscience Program, Institut d'Investigació Biomèdica de Bellvitge, IDIBELL, 08907 L'Hospitalet de Llobregat, Spain*
[c] *Institut d'Investigacions Biomèdiques de Barcelona (IIBB-CSIC), 08036 Barcelona, Spain*
[d] *Department of Biomedicine, School of Medicine and Health Sciences, Institute of Neurosciences, University of Barcelona, 08036 Barcelona, Spain*
[e] *Centro de Investigación Biomédica en Red de Salud Mental (CIBERSAM), ISCIII, 28029 Madrid, Spain*
[f] *Universitat de Vic-Universitat Central de Catalunya (UVic-UCC), Institut de Recerca i Innovació en Ciències de la Vida i de la Salut a la Catalunya Central (IRIS-CC), 08500 Vic, Spain*
[g] *Instituto de Biomedicina y Biotecnología de Cantabria (IBBTEC), Consejo Superior de Investigaciones Científicas (CSIC)-Universidad de Cantabria, 39011 Santander, Spain*
[h] *Institut d'Investigacions Biomèdiques August Pi i Sunyer (IDIBAPS), 08036 Barcelona, Spain*
[i] *Centro de Investigación Biomédica en Red Sobre Enfermedades Neurodegenerativas (CIBERNED), 28029 Madrid, Spain*
[j] *CNC-Center for Neuroscience and Cell Biology of Coimbra, University of Coimbra, 3004-504 Coimbra, Portugal*
[k] *FMUC-Faculty of Medicine, University of Coimbra, 3004-504 Coimbra, Portugal*
[l] *Center for Innovative Biomedicine and Biotechnology (CIBB), University of Coimbra, 3000-548 Coimbra, Portugal*

A R T I C L E I N F O

Keywords:
Cannabinoid
Δ^9-tetrahydrocannabinol
Cannabidiol
Alzheimer
Glutamate
Hippocampus

A B S T R A C T

A combination of Δ^9-tetrahydrocannabinol (Δ^9-THC) and cannabidiol (CBD) at non-psychoactive doses was previously demonstrated to reduce cognitive decline in APP/PS1 mice, an animal model of Alzheimer's disease (AD). However, the neurobiological substrates underlying these therapeutic properties of Δ^9-THC and CBD are not fully understood. Considering that dysregulation of glutamatergic activity contributes to cognitive impairment in AD, the present study evaluates the hypothesis that the combination of these two natural cannabinoids might reverse the alterations in glutamate dynamics within the hippocampus of this animal model of AD. Interestingly, our findings reveal that chronic treatment with Δ^9-THC and CBD, but not with any of them alone, reduces extracellular glutamate levels and the basal excitability of the hippocampus in APP/PS1 mice. These effects are not related to significant changes in the function and structure of glutamate synapses, as no relevant changes in synaptic plasticity, glutamate signaling or in the levels of key components of these synapses were observed in cannabinoid-treated mice. Our data instead indicate that these cannabinoid effects are associated with the control of glutamate uptake and/or to the regulation of the hippocampal network. Taken together, these results support the potential therapeutic properties of combining these natural cannabinoids against the excitotoxicity that occurs in AD brains.

* Corresponding author.
E-mail address: ester.aso@ub.edu (E. Aso).

https://doi.org/10.1016/j.neurot.2024.e00439
Received 25 April 2024; Received in revised form 13 August 2024; Accepted 16 August 2024

Introduction

Alzheimer's disease (AD) is characterized by an initial memory impairment and a progressive loss of other cognitive and mental abilities, affecting one in nine people over 65 years of age [1]. Considering the increased incidence of AD expected for the next few years [1] and the modest, if any, clinically significant benefit of the current therapies against AD [2,3], there is an urgent need to develop new agents designed to prevent or to curb the progression of AD. Among the potential novel therapeutic strategies against AD, cannabinoid compounds have attracted a growing interest during the last fifteen years because they might offer a multi-faceted approach to the treatment of AD. Cannabinoid receptors are highly expressed in the brain and, when targeted by endogenous ligands such as 2-arachidonoyl glycerol (2-AG) and anandamide (AEA) or cannabis derivatives including Δ^9-tetrahydrocannabinol (Δ^9-THC) and cannabidiol (CBD), provide neuroprotection by reducing neuronal damage, neuroinflammation and oxidative stress, as well as by modulating neurotransmission and promoting intrinsic repair mechanisms [4,5]. This pleiotropic activity of cannabinoid receptors sustains their interest as potential targets for AD and other neurodegenerative diseases [6,7]. Consistent with this hypothesis, our previous results revealed that the combination of non-psychoactive doses of Δ^9-THC and CBD, which are the main components of a cannabis-based medicine (nabiximols or Sativex®) already approved for other indications, reduces cognitive decline in a mouse model of AD (double transgenic APP/PS1 mice) more efficiently than each compound alone [8,9].

However, the molecular mechanisms underlying these therapeutic properties of Δ^9-THC and CBD are not fully understood. Δ^9-THC is a partial agonist of cannabinoid CB_1 and CB_2 receptors (CB_1R and CB_2R), while CBD acts on multiple targets beyond cannabinoid receptors [10]. To date, we have ruled out the possibility that CB_2R plays a major role in the therapeutic properties of Δ^9-THC and CBD in APP/PS1 mice, as the genetic deletion of this receptor did not impact on the cognitive improvement induced by chronic treatment with these cannabinoids in this AD model [11]. Our previous results indicated that the chronic administration of these compounds reduced the levels of soluble $A\beta_{1\text{-}42}$ peptide, the most toxic form of the amyloid-beta (Aβ) peptides, and also decreased inflammatory processes triggered by this peptide [8,9]. Soluble Aβ peptide overproduction is known to underlie synaptic dysfunction in AD [12], predominantly affecting glutamatergic terminals in the hippocampus [13,14] and consequently promoting neuronal hyperexcitability at early stages of the disease [15]. This imbalance of the neuronal network in the hippocampus leads to cognitive decline and increased susceptibility to seizures in AD patients and animal models of AD [16,17]. On the other hand, previous reports have demonstrated a key role for cannabinoid receptors in the control of neuronal excitability and epileptiform seizures in other conditions [18,19], as well as a contribution of altered 2-AG signaling in hippocampal glutamatergic synapses to the cognitive decline in AD patients [20]. Thus, we hypothesize that the Δ^9-THC and CBD combination could reduce the impact of the soluble Aβ peptide on excitatory neurotransmission and modulate the enhanced excitability state in APP/PS1 mice. To elucidate this question, the present study aims to evaluate in APP/PS1 mice the effects of the combination of Δ^9-THC and CBD on extracellular glutamate dynamics and on certain forms of neuronal plasticity previously demonstrated to be dependent on excitatory/inhibitory balance in the hippocampus, a key brain area related to cognitive processes and affected early in AD progression [21].

Materials and Methods

Animals

Male and female APP/PS1 mice and *wild-type* (WT, C57Bl/6j background) littermates aged 6 months at the beginning of the treatment were used for the study. The generation of mice expressing the human mutated APPswe and PS1dE9 has been described elsewhere [22]. Animals were housed in conventional polycarbonate cages, grouped 3–4 per cage in mixed-genotype conditions and maintained under standard animal housing conditions in a 12-h dark-light cycle with free access to food and water. Environmental enrichment included nesting material. The genotype of the animals was analyzed with the polymerase chain reaction technique using genomic DNA isolated from ear clips obtained after postnatal day 21. Mice were randomly assigned to treatment groups and the experiments were conducted under experimental blind conditions. All animal procedures were carried out by following the ARRIVE guidelines and the European Communities Council Directive 2010/63/EU, with the approval of the local ethical committees of the University of Barcelona (Authorization number 11206) and the Center for Neuroscience and Cell Biology-Coimbra (ORBEA_138/15072016). All efforts were made to minimize animal suffering and the number of animals used.

Pharmacological treatment

Δ^9-THC and CBD were purchased from Sigma-Aldrich (Merck, Sant Louis, MO, USA) and Tocris Bioscience (Bristol, UK), respectively, and were dissolved in 5% ethanol, 5% Tween and 90% saline. The combination of Δ^9-THC + CBD (0.5 mg/kg each), Δ^9-THC (0.5 mg/kg), CBD (0.5 mg/kg) or vehicle (VEH) were injected intra-peritoneally in a volume of 10 mL/kg body weight once a day for 5 weeks. The doses and treatment period are based on our previous studies reporting cognitive improvement in APP/PS1 mice [8,9].

In vivo microdialysis procedure and glutamate quantification

Extracellular glutamate concentrations were measured by *in vivo* intracerebral microdialysis in freely moving mice as previously described by our group [23,24]. The day after the end of the chronic treatment (to avoid a potential acute effect of the compounds on the surgery procedure or on the recovery period after the anesthetics), mice were anesthetized with isofluorane (5% induction, 1.5% maintenance) and placed in a stereotaxic apparatus with a flat skull. A small hole was drilled in the skull and a concentric dialysis probe with a 2-mm long membrane (Medicell Membranes Ltd, London, UK) was implanted directly in the right hippocampus (AP, −3.0 mm; ML, −2.7 mm; DV, −2.8 mm from bregma) according to the reference atlas [25], and then fixed to the skull with dental cement and two anchor screws. One day after probe implantation, freely moving animals were habituated to the experimental environment and the dialysis system was stabilized during 3 h by continuously perfusing probes with artificial cerebrospinal fluid (aCSF1: 125 mM NaCl, 2.5 mM KCl, 1.2 mM $CaCl_2$, 1.2 mM $MgCl_2$) at a constant rate of 1.5 µL/min with a CMA 402 syringe pump (CMA Microdialysis AB, Kista, Sweden) attached to a low-torque dual channel swivel (Instech, Plymouth Meeting, PA, USA). After stabilization, four consecutive 20-min dialysis samples were collected for the determination of baseline glutamate levels. Then, the voltage-gated sodium channels activator veratridine (50 µM) was administered for 20 min through the dialysis probe by reverse microdialysis and the collection of samples was continued for additional 80 min after administration. On the second day after probe implantation, 4 consecutive basal dialysis samples were collected after stabilization and before infusing the glutamate transporter 1 (GLT-1) inhibitor dihydrokainic acid (DHK, 5 mM) for 2 h 20-min dialysis samples were collected during the entire procedure. Glutamate concentrations in hippocampal samples were determined by high-performance liquid chromatography (HPLC) with fluorimetric detection. The HPLC system consisted of a Waters 717plus autosampler, a Waters 600 quaternary gradient pump, and a Nucleosil 5-µm ODS column (10 cm × 0.4 cm; Teknokroma, Spain). Dialysate samples were pre-column derivatized with OPA reagent and all this process was carried out by the autosampler. Briefly, 90 µL distilled water was added to a 10 µL dialysate sample and this was followed by the addition of 15 µL of the OPA reagent. After 2.5 min reaction, 80 µL of this mixture was injected

into the column. Detection was carried out with a Waters 470 Scanning Fluorescence Detector using excitation and emission wavelengths of 360 and 450 nm, respectively. The mobile phase consisted of 0.1 M sodium acetate, 5.5 mM triethylamine (pH 5.5) containing 10–70% acetonitrile and was pumped at 0.8 mL/min. The percentage of glutamate concentrations after veratridine or DHK challenge was calculated over basal concentrations through an area under the curve (AUC) using a standard trapezoid method [26]. The following equation was used: AUC = [0.5*(B + C_1)*d + 0.5*(C_1 + C_2)*d + 0.5* (C_2 + C_3)*d + … 0.5*(C_{n-1} + C_n)*d)], where B is the average basal value, C_1 to C_n are values during drug challenge, and d is the duration of the sample (20 min in this case). At the end of the experiments, animals were sacrificed, and brains were quickly removed. One hemisphere was dissected on ice, immediately frozen, and stored at −80 °C until used for protein determinations. The other hemisphere was fixed in 4% paraformaldehyde and processed for immunohistochemistry and hematoxilin staining to confirm the probe placement. Only those animals with correct probe placements were used in the study.

Gel electrophoresis and western blotting

Hippocampal samples were homogenized in 50 mM Tris-HCl buffer (pH 7.4) containing protease and phosphatase inhibitors (Roche Molecular Systems, Pleasanton, CA, USA). The homogenates were centrifuged for 10 min at 1000 *g* to remove cellular debris. The supernatant was recovered and centrifuged at 16100 *g* for 30 min. The pellet was used as membrane protein samples and the supernatant as cytosolic fractions. All samples were kept on ice and centrifugations were performed at 4 °C. Protein concentration was determined with the BCA method (Thermo Scientific, Waltham, MA, USA). Equal amounts of protein (10 μg) for each sample were loaded and separated by electrophoresis on sodium dodecyl sulfate polyacrylamide gel electrophoresis (SDS-PAGE) (10%) gels and transferred onto PVDF membranes (Millipore, Burlington, MA, USA). Non-specific binding was blocked by incubation in 3% albumin (VWR lnternational Eurolab, Llinars del Vallès, Spain) in PBS containing 0.05% Tween for 1 h at room temperature. Membranes were incubated overnight at 4 °C with the primary antibodies against AMPAR subunit GluA1 (1:1000, MAB2263, Millipore), NMDAR subunit GluN1 (1:1000, ab109182, Abcam, Cambridge, UK), metabotropic glutamate type 5 receptor (1:1000, mGlu5R) (Af-300, Nittobo Medical, Chiyoda-ku, Tokyo, Japan), phospho-eEF2 (1:1000, Thr56) (#2331, Cell Signalling, Danvers, Massachusetts, USA), eEF2 (1:1000, #2332, Cell Signalling), Fyn (pY528)/c-Src(pY530) (1:2500, 612668, BD Transduction Laboratories, Franklin Lakes, NJ, USA), Fyn (610163, BD Transduction Laboratories), EAAT3 (1:1000, 12686-1-AP, Proteintech, Rosemont, IL, USA), GLT-1 (1:2000, AB1783, Millipore). Membranes were then incubated for 1 h with the appropriate horseradish peroxidase (HRP)-conjugated secondary antibodies and immunocomplexes were revealed using a chemiluminescence reagent (Immobilon, Merck). Protein loading was monitored using an antibody against β-tubulin-HRP (1:2000, ab21058, Merck). Densitometric quantification was carried out with ImageJ software (NIH, Bethesda, MA, USA).

Electrophysiological recordings

Another batch of 6-months old WT and APP/PS1 mice chronically treated with VEH or Δ^9-THC + CBD was used for the electrophysiological recordings, essentially carried out as previously described [27]. After brief anesthesia under halothane or isoflurane atmosphere, mice were sacrificed by decapitation and their brain was quickly removed and placed in ice-cold, oxygenated (95% O_2, 5% CO_2) aCSF (aCSF2: 124 mM NaCl, 3 mM KCl, 1.25 mM Na_2HPO_4, 26 mM $NaHCO_3$, 2 mM $CaCl_2$, 1 mM $MgCl_2$, 10 mM glucose). Slices (400 μm-thick) were cut transverse to the long axis of the hippocampus using a McIlwain tissue chopper and allowed to recover in gassed aCSF for 1 h at 32 °C and another 40 min at room temperature. A slice from the dorsal hippocampus was then transferred to a submerged recording chamber and continuously perfused with gassed aCSF2 (3 mL/min). The stimulation was performed using either a Grass S44 or a Grass S48 square pulse stimulator (Grass Technologies, RI, USA), every 20 s with rectangular pulses of 0.1 ms, delivered through a bipolar concentric electrode placed in the proximal CA1 stratum radiatum for stimulation of the Schaffer collaterals. The extracellular recording of field excitatory post-synaptic potentials (fEPSP) was performed with a glass recording electrode, filled with 4 M NaCl (1–2 MΩ resistance), that was placed in the CA1 stratum radiatum targeting the distal dendrites of pyramidal neurons. After amplification (ISO-80, World Precision Instruments, Hertfordshire, UK), the recordings were digitized (BNC-2110, National Instruments, Newbury, UK), averaged in groups of 3, and analyzed using the WinLTP version 2.10 software (WinLTP Ltd., Bristol, UK). The intensity of stimulation was chosen between 30 and 50% of maximal fEPSP response, determined on the basis of input/output curves in which the fEPSP slope was plotted versus stimulus intensity. Long-term potentiation (LTP) was induced by high frequency stimulation (HFS) consisting of one train of 100 Hz pulses for 1 s or by a Theta-Burst Stimulation (TBS) consisting of 10 bursts of four pulses of 100 Hz with an inter-burst interval of 200 ms, repeated seven times at 0.03 Hz. The magnitude of LTP was calculated by comparing the average of fEPSP slopes between 50 and 60 min after HFS/TBS train with the average of the fEPSP slopes in the 10 min before the HFS/TBS (baseline). Paired-pulse facilitation ratio (PPF) was calculated as the ratio of the fEPSP slopes evoked by two consecutive pulses (ratio of P2/P1) with inter-pulse intervals of 25, 50 or 100 ms.

Fiber photometry for glutamate evaluation in anesthetized mice

Animals were anesthetized with 4% isoflurane and maintained at 1.5% isoflurane during stereotaxic surgery. Ears and mouth were fixed to maintain mouse head in place, and skull was exposed and perforated with a microdrill to allow viral vector injection. 300 nL of pssAAV-5/2-hSyn1-SF_iGluSnFR(A184S)-WPRE-SV40p(A) glutamate biosensor (iGluSnFR, 5.3×10^{12} vg/mL, v350, ETH Viral Vector Facility, University of Zurich, Switzerland) was infused into ventral hippocampus (AP -3 mm; ML -2.7 mm from bregma; DV -3 mm from skull). Injections were performed using a 2 μL microsyringe (Hamilton Neuros, Giarmata, Romania) and a syringe pump (Quintessential Stereotaxic Injector, Stoelting, USA) at 100 nL/min. After infusion, the microsyringe was left in place for 5 min to allow proper diffusion. Four to six weeks after viral vector transduction (1 day after the end of chronic treatment for treated animals), mice were anesthetized (4% isoflurane induction, 1.5% maintenance) and placed in the stereotaxic apparatus for acute fiber photometry recordings. An optic fiber cannula (4.5 mm, 400 μm core diameter and 0.5 NA) (RWD Life Science) was attached to a bipolar electrode (Plastics One Inc, Virginia, USA) and placed over the viral delivery area. Photometry data acquisition was performed at a sampling rate of 1204 samples per second with Doric Fiber Photometry Console and Neuroscience Studio V6 (Doric Lenses, Quebec, Canada). Changes in glutamate levels were recorded as variations in fluorescence emission at 500–550 nm, based on excitation by light source at 460–490 nm. The emission light was optically filtered and registered using the built-in photodetectors of the Doric Minicubes (5 ports Fluorescence Mini Cube, Doric). Digital data was low-pass filtered (10 Hz) and downsampled (10x). Then, mice were subjected to an electrical stimulation protocol consisting in 200 ms sequences of 2 ms pulses of 4 mA, delivered at increasing frequencies of stimulation (10 Hz–100 Hz) with an inter event interval of 1 min. Photometry signals were processed using MATLAB. Briefly, raw signal was normalized to correct fluorescence decay by fitting the decay to a biexponential equation (F_0), using the formula $dF/F_0=(F_{raw}-F_0)/F_0$. The corrected signal was then analyzed to isolate glutamate elicited peaks using the MATLAB function *findpeaks* and to quantify the amplitude of the peaks (dF/F_0 normalized to 100 Hz) and the decay time (time to return to the 90% of the baseline) using custom MATLAB codes. At the end the recordings, mice were sacrificed, brains immediately removed and fixed in 4%

paraformaldehyde. Then, brains were sliced for viral vector expression confirmation by fluorescence microscopy. Animals without proper or misplaced viral vector expression were excluded from the analysis.

DiI ballistic staining of dendritic spines

Hippocampal neurons from fixed brains of WT and APP/PS1 mice treated with Δ^9-THC + CBD or VEH were labeled using the Helios Gene Gun System (165–2431, Bio-Rad, Hercules, CA, USA). A suspension containing 3 mg of DiI (Molecular Probes, Eugene, OR, USA) dissolved in 100 µL of methylene chloride (Sigma-Aldrich) and mixed with 50 mg of tungsten particles (1.7 mm diameter; Bio-Rad) was spread on a glass slide and air-dried. The mixture was resuspended in 8 mL distilled water and sonicated. Subsequently, the mixture was placed into Tefzel tubing (Bio-Rad) and then removed to allow tube drying during 5 min under nitrogen gas flow. The tube was then cut into 13-mm pieces to be used as gun cartridges. Coronal sections (200 µm thick) of paraformaldehyde-fixed brain samples were shot at 80 psi through a membrane filter with 3 µm pore size and 8 × 10 pores/cm^2 (Millipore, Burlington, MA, USA) to deliver dye-coated particles in the hippocampus. Sections were mounted in Everbrite hardset mounting medium (VWR). CA1 hippocampal pyramidal neurons were imaged using a Zeiss LSM880 confocal microscope (Carl Zeiss AG, Jena, Germany). The spine density and morphology were examined in DiI-labeled segments of apical secondary dendrites of CA1 hippocampal pyramidal neurons. Confocal z-stacks including the entire volume of the dendrite were taken with a lateral resolution of 1024 × 1024 pixels. Quantification was conducted under blind experimental conditions using ImageJ. Spines were classified as stubby, mushroom, filopodia, thin or branched depending on their morphology [28].

Statistics

Data are presented as mean ± standard error of mean (SEM) with statistical significance set at $P < 0.05$. The number of samples (n) in each experimental condition is indicated in the legend of the corresponding figure. All the comparisons were performed using three-way factor analysis of variance (ANOVA) with sex, genotype and treatment as between factors followed by Tukey's multiple comparisons *post hoc* test when interaction between any factors was significant, except for the input-output curve in which a three-way ANOVA with genotype and treatment as between factors and stimulus intensity as repeated measures was applied considering male and female mice in the same experimental groups. In all the cases, GraphPad Prism 9 software was used for statistical analysis.

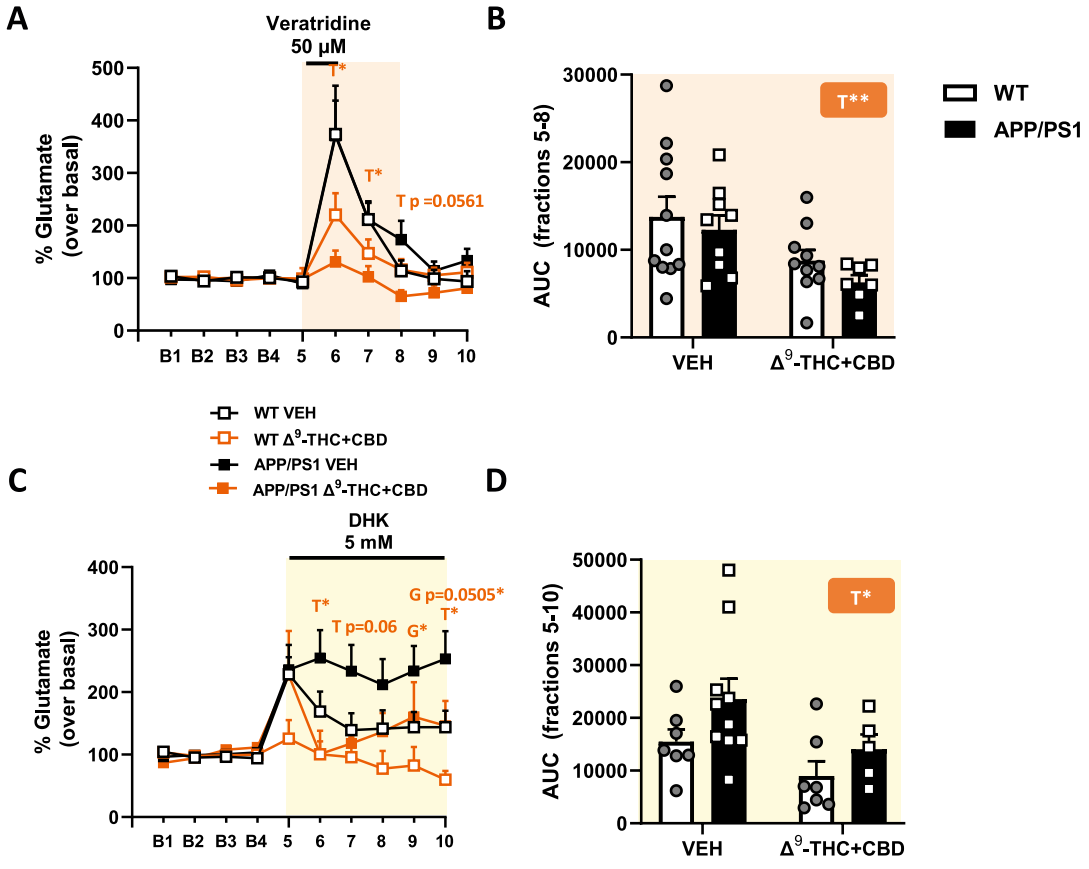

Fig. 1. Extracellular glutamate levels in the hippocampus of chronically treated WT and APP/PS1 mice measured by *in vivo* microdialysis. **(A)** Chronic treatment with Δ^9-THC + CBD (orange symbols) significantly decreased glutamate extracellular levels when compared to vehicle (VEH)-treated animals (white symbols) after the 20 min infusion with the depolarizing agent veratridine (50 µM) on fractions 6 and 7. **(B)** Area under the curve (AUC) values for the glutamate extracellular levels after veratridine infusion from fraction 5 to 8 (colored area in A) revealed a similar treatment effect. **(C)** Infusion during 2 h with the GLT-1 inhibitor DHK (5 mM) increased hippocampal glutamate extracellular levels, an increase significantly lower in mice chronically treated with Δ^9-THC + CBD (orange symbols) than in VEH-treated (white symbols) mice at fractions 6, 7 and 10. A genotype effect was also significant in fractions 9 and 10. **(D)** AUC values for the glutamate extracellular levels after DHK infusion from fraction 5 to 10 (colored area in C), revealing a similar treatment effect. Data are expressed as mean ± SEM (WT VEH n = 7 males + 4 females; WT Δ^9-THC + CBD n = 6 males + 8 females; APP/PS1 VEH n = 4 males + 5 females; APP/PS1 Δ^9-THC + CBD n = 2 males + 5 females). T*: Treatment effect, $p < 0.05$; T**: Treatment effect, $p < 0.01$; G*: Genotype effect, $p < 0.05$. (For interpretation of the references to color in this figure legend, the reader is referred to the Web version of this article.)

Results

Chronic combined treatment with Δ^9-THC and CBD reduces extracellular glutamate levels in the hippocampus of WT and APP/PS1 mice

We evaluated the extracellular glutamate levels in the hippocampus of WT and APP/PS1 mice chronically treated with Δ^9-THC + CBD or vehicle after the exposure to drugs known to increase the glutamate levels in the synapses. Three-way ANOVA revealed a significant effect of chronic treatment (fraction 6 and 7, $p < 0.05$; fraction 8, $p = 0.056$; AUC, $p < 0.01$), but without genotype or sex effect or interaction between factors, in the increased extracellular glutamate levels induced by the depolarizing agent veratridine perfused for 20 min in the hippocampus of mice (Fig. 1A–B). Regarding the results obtained in the hippocampal extracellular glutamate levels of chronically treated animals during the perfusion of the GLT-1 inhibitor DHK (Fig. 1C–D), three-way ANOVA revealed a significant genotype (fraction 10, $p < 0.05$; AUC, $p = 0.050$) and treatment effects (fraction 6 and AUC, $p < 0.05$; fraction 7, $p = 0.069$), but no sex effect or interaction between factors. Statistical details are included in Supplementary Table 1.

Δ^9-THC or CBD alone are not effective therapies to reduce the extracellular glutamate levels in the hippocampus of APP/PS1 mice

To evaluate the specific contribution of Δ^9-THC and CBD in the effects observed on glutamate levels in mice chronically treated with the combination of both natural cannabinoids, we performed similar *in vivo* microdialysis experiments in WT and APP/PS1 chronically treated only with Δ^9-THC or CBD. Our results revealed that neither Δ^9-THC (Supplementary Fig. 1) nor CBD (Supplementary Fig. 2) administered alone were able to reduce the increase induced by veratridine and/or DHK in extracellular glutamate levels in mice. In fact, chronic exposure to Δ^9-THC induced the opposite effect than the observed after the administration of the Δ^9-THC and CBD combination. Thus, a significant treatment effect (fraction 7 and AUC, $p < 0.01$; fraction 8, $p = 0.07$) on the glutamate levels in the hippocampus of mice during the perfusion with veratridine (Supplementary Fig. 1A and B) was observed. Moreover, a genotype effect (fraction 7, $p < 0.01$) and an interaction between genotype and treatment (fractions 5, 6, 8, 9, 10 and AUC, $p < 0.05$) were observed in mice chronically treated with Δ^9-THC and perfused with DHK (Supplementary Fig. 1C and D). In the case of CBD, no significant effect of sex, genotype, treatment or interaction between factors was observed during veratridine perfusion (Supplementary Fig. 2A and B). In contrast, perfusion with DHK induced a significant sex (fractions 8, 9 and AUC, $p < 0.01$; fractions 7 and 10, $p < 0.05$), genotype (fractions 7 and 8, $p < 0.05$; fraction 9, $p < 0.01$; AUC, $p < 0.001$) and treatment (fraction 9, $p < 0.05$) effects and interaction between sex and genotype (AUC, $p < 0.01$), sex and treatment (fractions 8 and 9, $p < 0.05$), genotype and treatment (AUC, $p < 0.05$) and interaction between all three factors (fraction 5, $p < 0.05$) in those animals (Fig. 3D). Thus, Tukey's *post hoc* test revealed that chronic CBD treatment induced in female APP/PS1 mice a higher glutamate levels than in female WT littermates in response to DHK perfusion (AUC, $p < 0.001$). Statistical details are included in Supplementary Table 2 (Δ^9-THC) and 3 (CBD).

Hippocampal protein levels of different glutamate signaling components

We evaluated the protein levels of several components of the glutamate signaling in the hippocampus of mice chronically treated with the combination of Δ^9-THC and CBD. First, we quantified in the membrane fractions the levels of certain glutamate receptors and the two main glutamate transporters: the neuronal excitatory amino acid transporter 3 (EAAT3) and the GLT-1 (also known as EAAT2), which is mainly located in astroglial cells and is the target of the DHK used in the microdialysis experiments [29]. Two-way ANOVA revealed a significant treatment effect on EAAT3 levels ($p < 0.05$; Fig. 2A), but no significant genotype

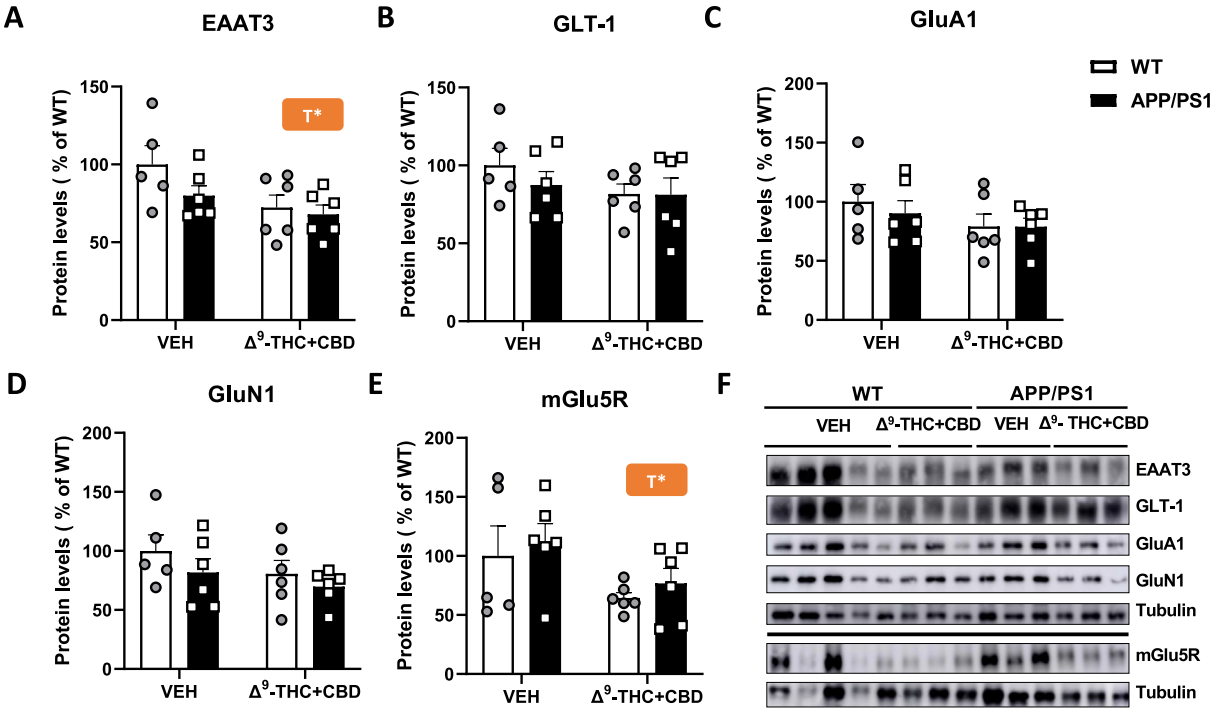

Fig. 2. **(A)** Representative immunoblots for EAAT3, GLT-1, GluA1, GluN1, mGlu5R and β-tubulin as loading control. Quantification by western blotting of the main glutamate transporters EAAT3 **(B)**, GLT-1 **(C)** and glutamate receptors subunits GluA1 **(D)**, GluN1 **(E)** and mGlu5R **(F)** in hippocampal samples from APP/PS1 (black bars) and WT (white bars) mice chronically treated with Δ^9-THC + CBD or vehicle (VEH). Densitometric quantifications of each protein are normalized respect β-tubulin and referred to vehicle-treated WT mice. **(F)** Individual values and mean ± SEM (WT VEH n = 2 males + 3 females; WT Δ^9-THC + CBD n = 4 males + 2 females; APP/PS1 VEH n = 3 males + 3 females; APP/PS1 Δ^9-THC + CBD n = 2 males + 4 females) are presented in the bar graphs. T*: Treatment effect, $p < 0.05$.

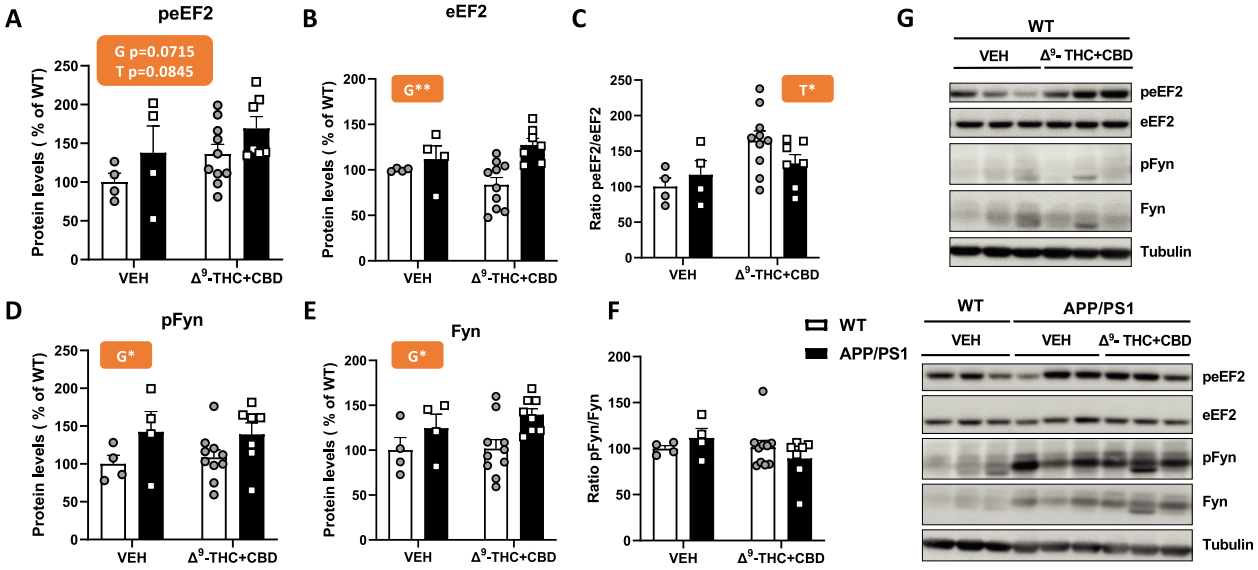

Fig. 3. **(A)** Representative immunoblots for peEF2, eEF2, pFyn, Fyn and β-tubulin as loading control. Quantification by western blotting of the phosphorylated and total forms of the glutamate signaling mediators eEF2 **(B–C)** and Fyn **(E–F)** in hippocampal samples from APP/PS1 (black bars) and WT (white bars) mice chronically treated with Δ^9-THC + CBD or vehicle (VEH). Densitometric quantifications of each protein are normalized respect β-tubulin and referred to vehicle-treated WT mice. **(D)** and **(G)** show the ratio between the phosphorylated and the total form of each signaling mediator. Individual values and mean ± SEM (WT VEH n = 3 males + 1 females; WT Δ^9-THC + CBD n = 5 males + 5 females; APP/PS1 VEH n = 2 males + 2 females; APP/PS1 Δ^9-THC + CBD n = 2 males + 5 females) are presented in the bar graphs. T*: Treatment effect, $p < 0.05$; G*: Genotype effect, $p < 0.05$; G**: Genotype effect, $p < 0.01$.

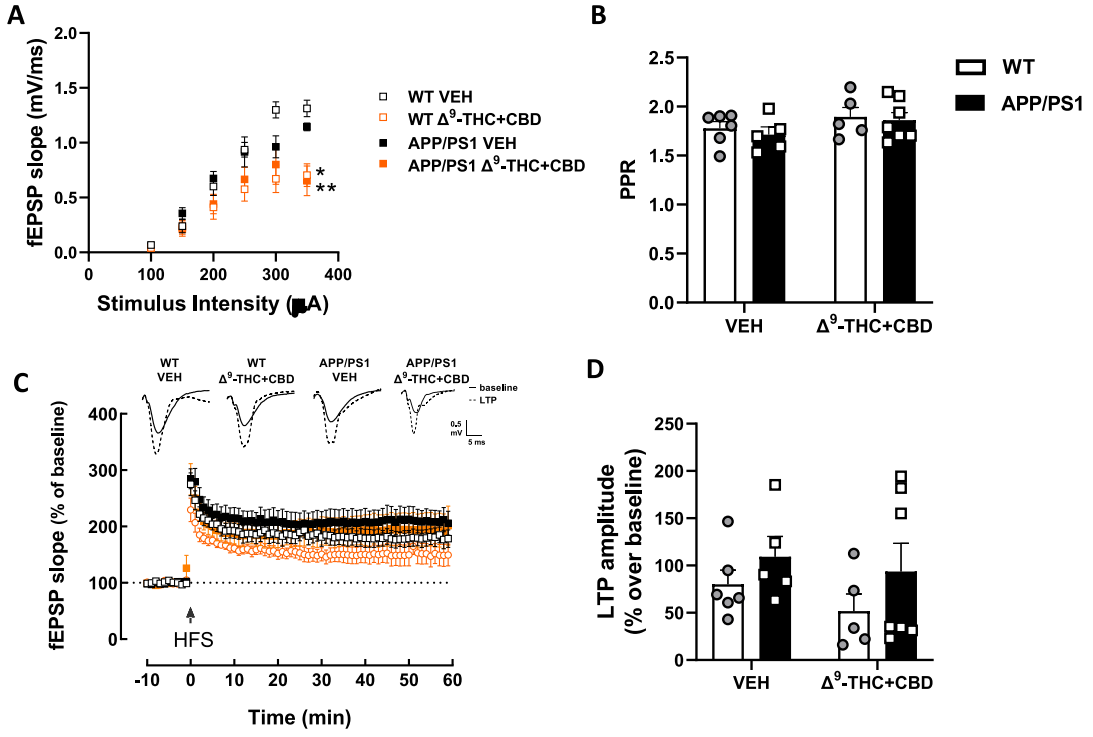

Fig. 4. **(A)** Input–output curves obtained in hippocampal slices of vehicle- (VEH) and Δ^9-THC + CBD-treated WT and APP/PS1 mice are displayed as the relationship between fEPSP slope (ordinates) and stimulus intensity (abscissa). Δ^9-THC + CBD chronic treatment induced a significant reduction in the maximum fEPSP slope in both genotypes. **(B)** Paired pulse ratio (PPR) showed a paired-pulse facilitation (PPR >1) with an interpulse interval of 50 ms with no differences between groups. **(C)** Time-course of the variation of the slope of fEPSPs, expressed as percentage of baseline values, in the CA1 stratum radiatum upon stimulation of afferent Schaffer collateral fibers, before and after induction of a long-term potentiation (LTP) with a train of high-frequency stimulation (HFS, 5 trains of 100 Hz for 1 s, arrow). No significant differences due to genotype or chronic treatment were observed. The inserts show representative recordings of the fEPSPs obtained for the indicated experimental groups. **(D)** Bar graph of LTP amplitude at 50–60 min after HFS. No significant differences due to genotype or chronic treatment were observed. Individual values and mean ± SEM (WT VEH n = 1 male + 5 females; WT Δ^9-THC + CBD n = 5 females; APP/PS1 VEH n = 3 males + 2 females; APP/PS1 Δ^9-THC + CBD n = 2 males + 5 females) are presented in the bar graphs. *$p < 0.05$, **$p < 0.01$ Tukey's *post hoc* test respect WT vehicle (VEH) group.

effect or interaction between factors. No genotype, treatment or interaction effects were observed on GLT-1 levels (Fig. 4B), or in the levels of the ionotropic glutamate AMPA and NMDA receptors subunits GluA1 and GluN1, respectively (Fig. 2C–D). In the case of the mGlu5R, two-way ANOVA revealed a significant treatment effect ($p < 0.05$) but no genotype or interaction between factors (Fig. 2E).

Next, we evaluated the NMDA- and mGlu5-dependent eukaryotic elongation factor 2 (eEF2) and the mGlu5-dependent Fyn pathways as glutamate signaling mediators in the cytosolic fraction of hippocampal samples from treated mice (Fig. 3). Two-way ANOVA revealed a significant genotype effect on total eEF2 levels (Fig. 3B, $p < 0.01$) and a tendency in the levels of phosphorylated eEF2 (Fig. 3A, $p = 0.0715$) but no treatment effect or interaction between both factors despite to a tendency to a treatment effect on phosphorylated eEF2 levels ($p = 0.0845$). Similarly, two-way ANOVA revealed a significant genotype effect in the levels of total and phosphorylated Fyn (Fig. 3D–E, $p < 0.05$) but without treatment effect or interaction between both factors. However, a significant treatment effect was observed in the ratio between the phosphorylated and total form of eEF2 (Fig. 3C, $p < 0.05$). Supplementary Table 4 includes all the statistical details related to the quantifications of the levels of the different proteins analyzed. Sex was not included as a between factor in the statistical analysis due to the limited number of samples from each sex included in the immunoblots.

Chronic combined treatment with Δ^9-THC and CBD reduces basal excitability but not synaptic plasticity in the hippocampus

Since synaptic plasticity of glutamatergic synapses is considered the neurophysiological basis of memory processes [30] and deficits of glutamatergic synapses and glutamatergic synaptic plasticity are present in animal models of AD [31], we evaluated the effects of the chronic combined treatment with the Δ^9-THC and CBD in basal synaptic transmission (Fig. 4A), in a short-term form of presynaptic plasticity (paired-pulse facilitation, PPF, Fig. 4B) and in a long-term form of synaptic plasticity (long-term potentiation, LTP, Fig. 4C–D) in the CA1-Schaffer collateral pathway in WT and APP/PS1 mice. In our experimental conditions, we did not observe any significant genotype-related differences in either basal synaptic transmission (assessed as input-output curve, Fig. 4A), PPF (Fig. 4B) or in the magnitude of LTP induced by HFS (Fig. 4C–D) or TBS (data not shown). Interestingly, chronic treatment reduced the maximum fEPSP slope of the input-output curve in both genotypes, suggesting a reduction in the proportion of synapses activated when the highest stimulus intensities were applied (Fig. 4A). Thus, three-way ANOVA revealed significant effects of stimulus intensity ($F_{(5, 87)} = 136.7$, $p < 0.001$), treatment ($F_{(1, 20)} = 13.54$, $p < 0.01$) and interaction between stimulus intensity, treatment and genotype ($F_{(5, 87)} = 7.866$, $p < 0.0001$) and between stimulus intensity and genotype ($F_{(5, 87)} = 2.863$, $p < 0.05$), but no genotype effect or interaction between genotype and treatment or between stimulus intensity and genotype. Subsequent Tukey's *post hoc* tests revealed a significant reduction in the maximum fEPSP slope in WT ($p < 0.01$) and APP/PS1 ($p < 0.05$) treated with Δ^9-THC + CBD with respect to VEH-treated WT mice. No treatment effect or interaction between factors was observed in any other electrophysiological parameter evaluated.

Chronic combined treatment with the Δ^9-THC and CBD does not reverse the decreased dendritic spine density in male APP/PS1 mice

We analyzed the density and morphology of dendritic spines labeled with DiI in CA1 hippocampal pyramidal neurons of WT and APP/PS1 treated mice (Fig. 5A, representative images of the analyzed dendrites). Three-way ANOVA revealed a significant interaction between genotype and sex in the total dendritic spine density ($p < 0.01$). Tukey's *post hoc* test revealed a significant reduction in the dendritic spine density in female WT VEH when compared to male WT VEH littermates ($p < 0.05$) and in male APP/PS1 VEH mice ($p < 0.05$) when compared to male WT VEH littermates (Fig. 5B). The specific analysis for each type of spine revealed a significant genotype (mushroom-type spines, $p < 0.05$),

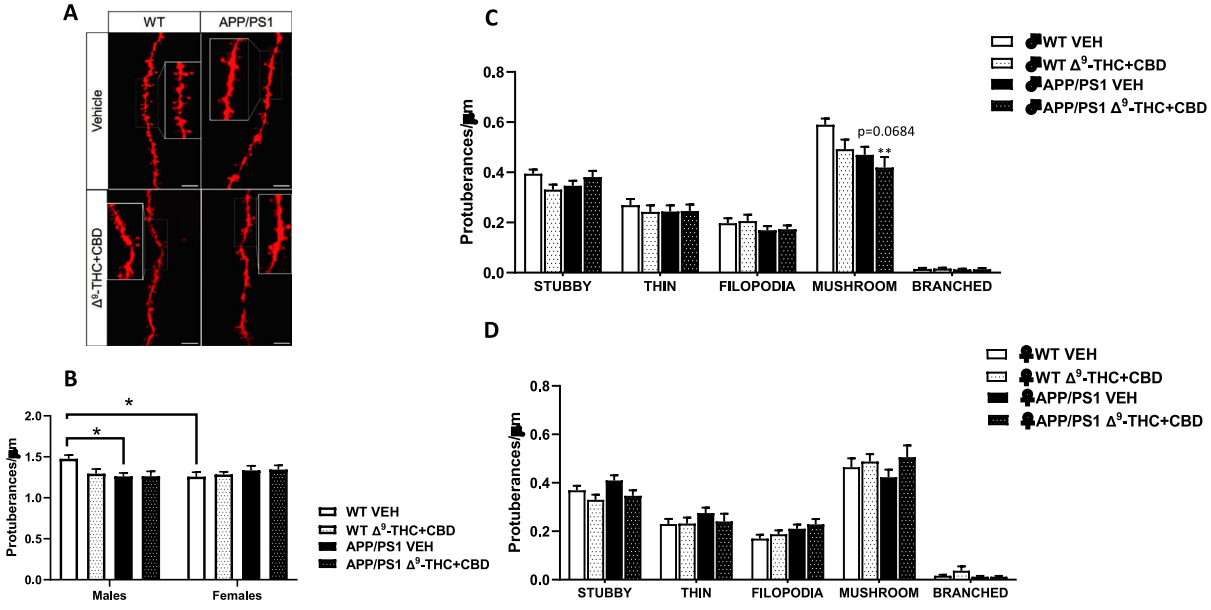

Fig. 5. **(A)** Representative dendrites of CA1 pyramidal neurons from vehicle- and Δ^9-THC + CBD-treated male WT and APP/PS1 mice. Scale bars represent 5 µm. **(B)** Quantitative analysis showing dendritic spine density per micrometer of dendritic length in CA1 pyramidal neurons from male and female WT and APP/PS1 mice at 6 months of age. A significant reduction in the dendritic spine density in female WT and male APP/PS1 mice was observed when compared to male WT littermates. **(C)** Density of each morphological type of dendritic spine in male treated mice. A significant decrease in the density of mushroom spines was observed in Δ^9-THC + CBD-treated APP/PS1 respect treated WT mice. **(D)** No significant differences due to genotype or treatment were observed in the total dendritic spine density in female treated mice, in spite of a significant treatment effect in the density of stubby spines. Data are expressed as mean ± SEM (n = 45–55 dendrites from WT VEH n = 4 males + 4 females; WT Δ^9-THC + CBD n = 4 males + 4 females; APP/PS1 VEH n = 4 males + 4 females; APP/PS1 Δ^9-THC + CBD n = 3 males + 3 females). *$p < 0.05$, **$p < 0.01$ respect control groups.

treatment (stubby-type spines, $p < 0.05$) effects and interaction between sex and genotype (filopodia, $p < 0.01$ and mushroom-type spines, $p < 0.05$), and between sex, genotype and treatment (stubby-type spines, $p < 0.05$). Subsequent Tukey's *post hoc* test revealed a tendency to a reduction in the mushroom-type spines ($p = 0.0684$) in VEH-treated APP/PS1male mice compared to VEH-treated male WT and a lower density of mushroom spines in Δ^9-THC + CBD-treated male APP/PS1 than in treated male WT mice ($p < 0.01$) (Fig. 5C). In female mice, no statistical differences between groups were observed (Fig. 5D). Supplementary Table 5 includes all the statistical details about dendritic spines analyses.

Glutamate uptake deficit in the hippocampus of APP/PS1 mice is reversed by chronic combined treatment with Δ^9-THC and CBD

We characterized the kinetics of electrically-evoked glutamate release in chronically treated WT and APP/PS1 mice using fiber photometry and the glutamate biosensor iGluSnFR. Three-way ANOVA revealed a significant effect of sex (30 Hz, $p < 0.05$; 40, 50, 60 and 80 Hz, $p < 0.01$), but not genotype or treatment effect, nor interaction between factors in the glutamate peak amplitude normalized to the maximum dF/F_0 signal (100 Hz) (Fig. 6B–C). In contrast, a significant genotype effect (30 Hz, $p < 0.05$) and an interaction between sex and treatment (30 Hz, $p < 0.01$; 80 Hz, $p < 0.05$) and between genotype and treatment (20, 30, 40, 50, 60, 80, 100 Hz, $p < 0.05$; 30 Hz, $p < 0.01$) were observed in the decay time of the peaks (Fig. 6B, D). Subsequent Turkey's *post hoc* test revealed a significant increase in the decay time in male APP/PS1 VEH mice when compared to APP/PS1 chronically treated with Δ^9-THC + CBD (30 Hz, $p < 0.05$, 80 Hz, $p = 0.0796$). Supplementary Table 6 includes all the statistical details related to the fiber photometry results. Comparisons between male and female are not included in Supplementary Table 6 because some experimental groups have a limited number of individuals of each sex and they are not the main focus of this study, but in all the cases there is a trend to higher decay time values in female than male mice.

Discussion

This study provides novel insights into the potential utility of the combination of the two main natural cannabinoids, Δ^9-THC and CBD, in AD-like conditions. Specifically, our data reveal that a chronic treatment with non-psychoactive doses of Δ^9-THC + CBD, when administered in combination but not individually, effectively reduces the increase in glutamate extracellular levels induced by the depolarizing agent veratridine and by the GLT-1 inhibitor DHK in the hippocampus of WT and, more importantly, of APP/PS1 mice. Moreover, the chronic Δ^9-THC + CBD treatment reduces the basal excitability of CA1 hippocampal synapses, as indicated by the lower maximum synaptic response achieved when recording the input/output response in Schaffer collaterals-CA1 synapses, and reverses the deficiencies in glutamate reuptake observed in transgenic mice. These findings could be of relevance considering that hippocampal hyperactivity has been associated with the neurodegenerative progression in AD animal models and patients [32–35]. Thus, mitigating glutamate-induced hippocampal hyperactivity might provide therapeutic benefits in AD.

Glutamatergic homeostasis in the central nervous system encompasses three key functional components, namely the pre- and post-

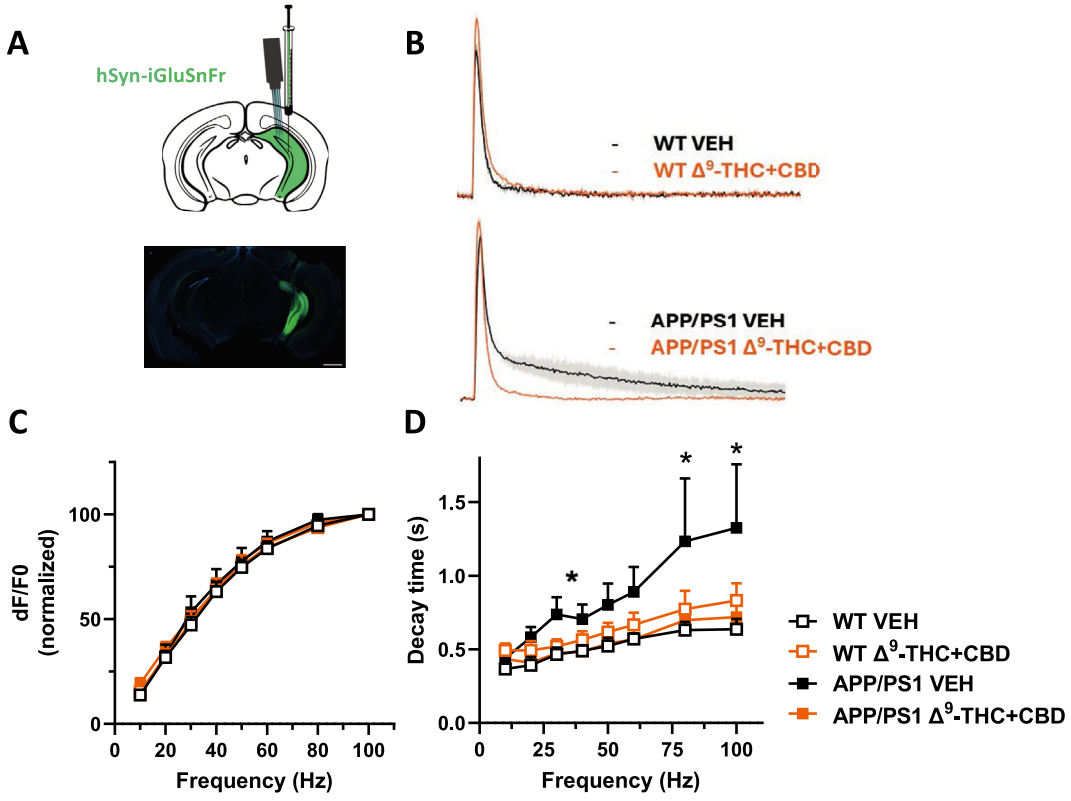

Fig. 6. (A) Diagram showing the ventral hippocampal area where glutamate biosensor (iGluSnFr) was injected and the optic fiber cannula attached to a bipolar electrode were placed for photometry recordings (upper panel). Lower panel shows a representative slide expressing iGluSnFr sensor. **(B)** Representative traces of iGluSnFR signal after electrical stimulation of the hippocampus in WT (upper panel) and APP/PS1 (lower panel) mice chronically treated with vehicle (VEH, black lines) or Δ^9-THC + CBD (orange lines). **(C)** Chronic treatment with Δ^9-THC + CBD did not affect dF/F_0 measurements for the elicited peaks at any frequency, but reversed the increased decay time observed in APP/PS1 treated with VEH (**D**). Data are expressed as mean ± SEM (WT VEH n = 4 male + 3 females; WT Δ^9-THC+CBD n = 5 male + 3 females; APP/PS1 VEH n = 2 males + 3 females; APP/PS1 Δ^9-THC+CBD n = 5 males + 4 females). *$p < 0.05$ respect APP/PS1 VEH group. (For interpretation of the references to color in this figure legend, the reader is referred to the Web version of this article.)

synaptic neuronal compartments along with glial cells, which are defined together as the tripartite synapse [36]. At the presynaptic level, glutamate neurotransmission can be regulated by modulating the vesicular glutamate transporters that store glutamate into vesicles and/or by regulating the mechanisms that mediate neurotransmitter release after neuronal depolarization. Our data on the reduced extracellular glutamate levels in response to veratridine and DHK in treated mice could be interpreted as an evidence for the ability of the Δ^9-THC + CBD treatment to mitigate neurotransmitter release from presynaptic glutamatergic terminals in the hippocampus. However, our electrophysiological recordings revealed that Δ^9-THC + CBD did not modify a form of short-term presynaptic plasticity (PPF) in either WT or APP/PS1 mice. In fact, an unaltered PPF reveals a preserved release probability, suggesting the lack of major presynaptic modifications that affect glutamate release between genotypes (WT *vs* APP/PS1 mice) or upon Δ^9-THC + CBD treatment. Thus, the decreased extracellular glutamate levels observed in the hippocampus of chronically treated mice could be instead a consequence of cannabinoid-induced modifications in the excitatory/inhibitory network regulating hippocampal activity, as suggested by the input/output response curves, in which we observed a reduction in the proportion of synapses recruited in response to a series of increasing electrical stimuli.

We also evaluated a long-term form of synaptic plasticity (i.e. LTP), which represents an intrinsic adaptive modification of glutamatergic synapses modification directly related to learning and memory. Unlike some previous reports [37,38], but consistent with others [39], we did not observe alterations in the magnitude of LTP in Schaffer collateral fibers-CA1 pyramidal synapses in APP/PS1 mice, regardless of chronic treatment with Δ^9-THC + CBD. This suggests that modifications in synaptic plasticity within the CA1 area in this AD model are inconsistent, which are probably strain-dependent [40], age-related [41,42] or depend on the proximity to amyloid plaques [43]. In line with the preserved LTP magnitude observed in APP/PS1, no major alterations of some postsynaptic components of glutamatergic signaling were observed in our experimental conditions. Specifically, we focused on the ionotropic AMPA and NMDA receptors, which are altered during AD progression [44], and the metabotropic mGlu5R, which can interact with Aβ oligomers to cause the disruption of normal glutamatergic activity that contributes to cognitive decline and excitotoxicity in AD brains [45]. Our immunoblotting results indicate that the chronic treatment with the combination of the natural cannabinoids did not alter the levels of the most common subunits of these receptors in the cell membrane nor their associated eEF2 or Fyn signaling pathways in APP/PS1 mice.

Dendritic spines are actin-rich protrusions where most excitatory synapses occur and whose density and morphology determine the strength and activity of the synapse, being consequently crucial in synaptic plasticity [46]. A decrease in dendritic spine density and alterations in its morphology have been observed in the hippocampus of certain AD models [47,48] and patients [49]. For these reasons, we performed an analysis of dendritic spine density and spine morphology in the CA1 hippocampal pyramidal neurons of mice chronically treated with Δ^9-THC + CBD. Interestingly, we observed a sex-dependent deficiency in dendritic spine density in APP/PS1 mice. Thus, only male APP/PS1 mice exhibited a reduced dendritic spine density in the hippocampal neurons as previously reported in other AD models [47,48]. The total dendritic spine density decrease observed in male APP/PS1 mice was mainly due to a reduction in the number of mushroom-type spines, which are considered more mature and stable structures [28]. However, chronic treatment with Δ^9-THC and CBD was unable to reverse this deficiency, reinforcing the suggestion that these cannabinoids have no direct effect on hippocampal synaptic plasticity in APP/PS1 mice.

In general, these findings indicate that the effects of the chronic treatment with Δ^9-THC + CBD in APP/PS1 mice are not linked to a direct control of glutamatergic synapses. Instead, these effects may be related to the regulation of hippocampal network activity. Thus, the effects of the chronic treatment with these cannabinoids on the increased levels of extracellular glutamate induced by the depolarizing agent veratridine both in WT and APP/PS1 mice suggest a reduction in the overall overexcitation of the neuronal network caused by Aβ peptides in the hippocampus [15], which in turn leads to glutamatergic excitotoxicity and ultimately to cognitive impairment [50]. An additional major finding of the present study was the ability of chronic treatment with the Δ^9-THC and CBD combination to control glutamate uptake depending on the activity of high-efficiency transporters located mainly on astrocytes but also in neurons [29]. Thus, our data reveal that the increase in the extracellular glutamate levels induced by the GLT-1 inhibitor DHK, which is tendentially higher in APP/PS1 mice, was significantly attenuated in mice chronically treated with the combination of Δ^9-THC and CBD. We discard that these effects were due to a direct effect of cannabinoid treatment on the levels of GLT-1. A slight decrease in the levels of EAAT3, the second most abundant glutamate transporter in the brain, was observed in the hippocampus of cannabinoid-treated mice. However, considering that GLT-1 accounts for around 95% of the total glutamate uptake activity in the brain [29], we consider that such an effect on EAAT3 levels could play a minor role in the modulation of the extracellular glutamate levels observed in mice chronically treated with Δ^9-THC and CBD. Thus, the results observed during the infusion with DHK support the hypothesis that the combination of Δ^9-THC and CBD critically controls the uptake of glutamate, likely by acting at the astrocytic level, thus regulating the extracellular levels of glutamate, and consequently impacting on the overall excitability of hippocampal networks rather than directly modifying glutamatergic synapses. To confirm this hypothesis, we performed fiber photometry experiments by using a glutamate biosensor, a technique with much higher temporal resolution than *in vivo* microdialysis. To gain control over glutamate temporal dynamics we performed local electrical stimulation on anesthetized mice. Remarkedly, chronic treatment with Δ^9-THC and CBD reversed the increased decay time of the electrically-induced glutamate peaks observed in APP/PS1 mice under basal conditions in the hippocampus, which instead reflects the system's capacity to re-uptake the glutamate released. Considering the robust data revealing how astrocytic activity affects hippocampal-dependent learning and memory deficits and its role in AD [51], as well as the increasing evidence about the presence and functional relevance of cannabinoid receptors in astrocytes [52], our data suggest that the cognitive benefits of the chronic treatment with Δ^9-THC and CBD in AD may rely on their action on astrocytes to control the glutamate dynamics. Additional experiments would be required to confirm this hypothesis and to identify the molecular mechanisms underlying such cannabinoids effects.

To note, our study provides additional evidence about the fact that the combination of Δ^9-THC and CBD exhibits a better therapeutic profile against AD than each cannabis component alone, as previous data indicated [8]. Thus, chronic treatment with either Δ^9-THC or CBD alone caused completely different effects than the combination of both on the extracellular glutamate levels in the hippocampus of WT and APP/PS1 mice. Specifically, Δ^9-THC induced higher extracellular glutamate levels in WT mice, while CBD induced an increase in glutamate levels in APP/PS1 mice during DHK infusion. Intriguingly, both Δ^9-THC and CBD appear to delay the veratridine-induced peak of extracellular glutamate. Further experiments will be required to find a mechanistic explanation for these findings and to explore the translational relevance that they could have for chronic consumption of purified extracts in healthy aging. Nevertheless, these results support a synergistic interaction between Δ^9-THC and CBD, as has been proposed for other cannabis derivatives [53], and underline the higher potential utility of multi-cannabinoid treatment strategies against AD [54].

Considering our present results, we can conclude that the chronic treatment with the combination of Δ^9-THC and CBD reduces extracellular glutamate levels and the basal excitability of the hippocampus in APP/PS1 mice. We excluded the possibility that the chronic treatment with Δ^9-THC and CBD could affect the function and structure of glutamate synapses. Our data instead suggest that these cannabinoid effects

could be related to the control of glutamate uptake, which is mainly carried out by astrocytes, and/or to the regulation of hippocampal network. These results support the potential therapeutic properties of the combination of these natural cannabinoids against the excitotoxicity occurring in AD brains and stimulate further research to untangle Δ^9-THC and CBD mechanisms of action.

Ethical approval

All animal experimental procedures were performed in accordance with Spanish (Real Decreto 53/2013), Portuguese (Decreto-Lei 113/2013) and European Union regulations (2010/63/UE) and were approved by the Ethical Committee for Animal Experimentation of the University of Barcelona and the Generalitat de Catalunya (authorization #11206), as well as by the Center for Neuroscience and Cell Biology of the University of Coimbra (ORBEA_138/15072016).

Availability of data and material

The datasets used and/or analyzed during the current study are available from the corresponding author on reasonable request.

Funding

This study was supported by Ministerio de Ciencia, Innovación y Universidades–Agencia Estatal de Investigación-FEDER funds/European Regional Development Fund – "a way to build Europe" grants RTI2018-097773-A-I00 and PID2022-141123OB-I00 to EA, PID2020-118511RB-I00 to FC, PID2020-119305RB-I00 to XG and PID2020-117989RA-I00 to JB, by Departament de Recerca i Universitats de la Generalitat de Catalunya (2021 SGR 00698) to FC and by CYTED-Programa Iberoamericano de Ciencia y Tecnología para el Desarrollo (P219RT0008) to EA. Founded by MCIN/AEI/10.13039/501100011033 "ESF Investing in your future" grant PRE2019-088153 to NSF and grant FPU19/03142 to LGA.

Author's Contributions

NSF and LGA participated in all the experiments, analyzed the results and contributed to the manuscript preparation. AC contributed to the *in vivo* microdialysis experiments and to the discussion of the results. AA and LC performed all the HPLC measurements and contributed to the interpretation of the results. JB contributed to setting up the fiber photometry technique and to the analysis of photometry results. VB and SG helped with the DiI ballistic labelling experiments and the discussion of the results. FQ, HS, JPL, CRL and MR performed the electrophysiology recordings. XG, RAC, AK and SF contributed to the discussion of the electrophysiology results and to the manuscript preparation. FC contributed to the discussion of all the results and to the manuscript preparation. EA conceived and designed the study and wrote the manuscript. All the authors read and approved the final manuscript.

Declaration of competing interest

The authors declare the following financial interests/personal relationships which may be considered as potential competing interests: Ester Aso reports financial support was provided by Spain Ministry of Science and Innovation. Jordi Bonaventura reports financial support was provided by Spain Ministry of Science and Innovation. Francisco Ciruela reports financial support was provided by Spain Ministry of Science and Innovation. Xavier Gasull reports financial support was provided by Spain Ministry of Science and Innovation. Francisco Ciruela reports financial support was provided by Departament de Recerca i Universitats de la Generalitat de Catalunya. Ester Aso reports financial support was provided by CYTED-Programa Iberoamericano de Ciencia y Tecnología para el Desarrollo. If there are other authors, they declare that they have no known competing financial interests or personal relationships that could have appeared to influence the work reported in this paper.

Acknowledgements

We thank Centres de Recerca de Catalunya (CERCA) Programme/Generalitat de Catalunya for IDIBELL institutional support and Maria de Maeztu MDM-2017-0729 to Institut de Neurociències, Universitat de Barcelona. We are also grateful to the CannaLatan network members (CYTED-Programa Iberoamericano de Ciencia y Tecnología para el Desarrollo) for the fruitful discussion about the results, and to Miquel Martín (Universitat Pompeu Fabra) for his kind advises about DiI ballistic labelling.

Appendix A. Supplementary data

Supplementary data to this article can be found online at https://doi.org/10.1016/j.neurot.2024.e00439.

References

[1] Alzheimer's Association. 2022 Alzheimer's disease facts and figures. Alzheimers Dement 2022;18.
[2] Howard R, McShane R, Lindesay J, Ritchie C, Baldwin A, Barber R, et al. Donepezil and memantine for moderate-to-severe Alzheimer's disease. N Engl J Med 2012;366:893–903.
[3] Liu KY, Walsh S, Brayne C, Merrick R, Richard E, Howard R. Evaluation of clinical benefits of treatments for Alzheimer's disease. Lancet Healthy Longev 2023;4:e645–51.
[4] Lu HC, Mackie K. An introduction to the endogenous cannabinoid system. Biol Psychiatr 2016;79:516–25.
[5] Solymosi K, Köfalvi A. Cannabis: a treasure trove or pandora's box? Mini Rev Med Chem 2017;17:1223–91.
[6] Aso E, Ferrer I. Cannabinoids for treatment of Alzheimer's disease: moving toward the clinic. Front Pharmacol 2014;5:37.
[7] Aymerich MS, Aso E, Abellanas MA, Tolón RM, Ramos JA, Ferrer I, et al. Cannabinoid pharmacology/therapeutics in chronic degenerative disorders affecting the central nervous system. Biochem Pharmacol 2018;157:67–84.
[8] Aso E, Sánchez-Pla A, Vegas-Lozano E, Maldonado R, Ferrer I. Cannabis-based medicine reduces multiple pathological processes in AβPP/PS1 mice. J Alzheimers Dis 2015;43:977–91.
[9] Aso E, Andrés-Benito P, Ferrer I. Delineating the efficacy of a cannabis-based medicine at advanced stages of dementia in a murine model. J Alzheimers Dis 2016;54:903–12.
[10] McPartland JM, Duncan M, Di Marzo V, Pertwee RG. Are cannabidiol and Δ(9)-tetrahydrocannabivarin negative modulators of the endocannabinoid system? A systematic review. Br J Pharmacol 2015;172:737–53.
[11] Aso E, Andrés-Benito P, Carmona M, Maldonado R, Ferrer I. Cannabinoid Receptor 2 Participates in amyloid-β processing in a mouse model of Alzheimer's disease but plays a minor role in the therapeutic properties of a cannabis-based medicine. J Alzheimers Dis 2016;51:489–500.
[12] Paula-Lima AC, Brito-Moreira J, Ferreira ST. Deregulation of excitatory neurotransmission underlying synapse failure in Alzheimer's disease. J Neurochem 2013;126:191–202.
[13] Canas PM, Simões AP, Rodrigues RJ, Cunha RA. Predominant loss of glutamatergic terminal markers in a β-amyloid peptide model of Alzheimer's disease. Neuropharmacology 2014;76:51–6.
[14] Rodríguez-Perdigón M, Tordera RM, Gil-Bea FJ, Gerenu G, Ramírez MJ, Solas M. Down-regulation of glutamatergic terminals (VGLUT1) driven by Aβ in Alzheimer's disease. Hippocampus 2016;26:1303–12.
[15] Targa Dias Anastacio H, Matosin N, Ooi L. Neuronal hyperexcitability in Alzheimer's disease: what are the drivers behind this aberrant phenotype? Transl Psychiatry 2022;12:257.
[16] Palop JJ, Chin J, Roberson ED, Wang J, Thwin MT, Bien-Ly N, et al. Aberrant excitatory neuronal activity and compensatory remodeling of inhibitory hippocampal circuits in mouse models of Alzheimer's disease. Neuron 2007;55:697–711.
[17] Irizarry MC, Jin S, He F, Emond JA, Raman R, Thomas RG, et al. Incidence of new-onset seizures in mild to moderate Alzheimer disease. Arch Neurol 2012;69:368–72.
[18] Lutz B. On-demand activation of the endocannabinoid system in the control of neuronal excitability and epileptiform seizures. Biochem Pharmacol 2004;68:1691–8.
[19] Monory K, Massa F, Egertová M, Eder M, Blaudzun H, Westenbroek R, et al. The endocannabinoid system controls key epileptogenic circuits in the hippocampus. Neuron 2006;51:455–66.
[20] Mulder J, Zilberter M, Pasquaré SJ, Alpár A, Schulte G, Ferreira SG, et al. Molecular reorganization of endocannabinoid signalling in Alzheimer's disease. Brain 2011;134:1041–60.
[21] Braak H, Braak E. Neuropathological stageing of Alzheimer-related changes. Acta Neuropathol 1991;82:239–59.

[22] Borchelt DR, Ratovitski T, van Lare J, Lee MK, Gonzales V, Jenkins NA, et al. Accelerated amyloid deposition in the brains of transgenic mice coexpressing mutant presenilin 1 and amyloid precursor proteins. Neuron 1997;19:939–45.
[23] López-Gil X, Artigas F, Adell A. Role of different monoamine receptors controlling MK-801-induced release of serotonin and glutamate in the medial prefrontal cortex: relevance for antipsychotic action. Int J Neuropsychopharmacol 2009;12:487–99.
[24] Tarrés-Gatius M, Miquel-Rio L, Campa L, Artigas F, Castañé A. Involvement of NMDA receptors containing the GluN2C subunit in the psychotomimetic and antidepressant-like effects of ketamine. Transl Psychiatry 2020;10:427.
[25] Paxinos G, Franklin KBJ. The mouse brain in stereotaxic coordinates. San Diego: Academic Press; 1997.
[26] Gibaldi M, Perrier D. Pharmacokinetics. New York: Dekker; 1975.
[27] Lopes CR, Silva JS, Santos J, Rodrigues MS, Madeira D, Oliveira A, et al. Downregulation of sirtuin 1 does not account for the impaired long-term potentiation in the prefrontal cortex of female APPswe/PS1dE9 mice modelling Alzheimer's disease. Int J Mol Sci 2023;24:6968.
[28] Hering H, Sheng M. Dendritic spines: structure, dynamics and regulation. Nat Rev Neurosci 2001;2:880–8.
[29] Danbolt NC, Furness DN, Zhou Y. Neuronal vs glial glutamate uptake: resolving the conundrum. Neurochem Int 2016;98:29–45.
[30] Kandel ER, Dudai Y, Mayford MR. The molecular and systems biology of memory. Cell 2014;157:163–86.
[31] Ondrejcak T, Klyubin I, Hu NW, Barry AE, Cullen WK, Rowan MJ. Alzheimer's disease amyloid beta-protein and synaptic function. NeuroMolecular Med 2010;12:13–26.
[32] Miller SL, Fenstermacher E, Bates J, Blacker D, Sperling RA, Dickerson BC. Hippocampal activation in adults with mild cognitive impairment predicts subsequent cognitive decline. J Neurol Neurosurg Psychiatry 2008;79:630–5.
[33] O'Brien JL, O'Keefe KM, LaViolette PS, DeLuca AN, Blacker D, Dickerson BC, et al. Longitudinal fMRI in elderly reveals loss of hippocampal activation with clinical decline. Neurology 2010;74:1969–76.
[34] Hascup KN, Findley CA, Sime LN, Hascup ER. Hippocampal alterations in glutamatergic signaling during amyloid progression in AβPP/PS1 mice. Sci Rep 2020;10:14503.
[35] Cox MF, Hascup ER, Bartke A, Hascup KN. Friend or foe? Defining the role of glutamate in aging and Alzheimer's disease. Front Aging 2022;3:929474.
[36] Lalo U, Koh W, Lee CJ, Pankratov Y. The tripartite glutamatergic synapse. Neuropharmacology 2021;199:108758.
[37] Trinchese F, Liu S, Battaglia F, Walter S, Mathews PM, Arancio O. Progressive age-related development of Alzheimer-like pathology in APP/PS1 mice. Ann Neurol 2004;55:801–14.
[38] Ma T, Chen Y, Vingtdeux V, Zhao H, Viollet B, Marambaud P, et al. Inhibition of AMP-activated protein kinase signaling alleviates impairments in hippocampal synaptic plasticity induced by amyloid β. J Neurosci 2014;34:12230–8.
[39] Song S, Wang X, Sava V, Weeber EJ, Sanchez-Ramos J. *In vivo* administration of granulocyte colony-stimulating factor restores long-term depression in hippocampal slices prepared from transgenic APP/PS1 mice. J Neurosci Res 2014;92:975–80.
[40] Sri S, Pegasiou CM, Cave CA, Hough K, Wood N, Gomez-Nicola D, et al. Emergence of synaptic and cognitive impairment in a mature-onset APP mouse model of Alzheimer's disease. Acta Neuropathol Commun 2019;7:25.
[41] Gengler S, Hamilton A, Hölscher C. Synaptic plasticity in the hippocampus of a APP/PS1 mouse model of Alzheimer's disease is impaired in old but not young mice. PLoS One 2010;5:e9764.
[42] Gelman S, Palma J, Tombaugh G, Ghavami A. Differences in synaptic dysfunction between rTg4510 and APP/PS1 mouse models of alzheimer's disease. J Alzheimers Dis 2018;61:195–208.
[43] Garad M, Edelmann E, Leßmann V. Impairment of spike-timing-dependent plasticity at schaffer collateral-CA1 synapses in adult APP/PS1 mice depends on proximity of aβ plaques. Int J Mol Sci 2021;22:1378.
[44] Findley CA, Bartke A, Hascup KN, Hascup ER. Amyloid beta-related alterations to glutamate signaling dynamics during Alzheimer's disease progression. ASN Neuro 2019;11:1759091419855541.
[45] Um JW, Kaufman AC, Kostylev M, Heiss JK, Stagi M, Takahashi H, et al. Metabotropic glutamate receptor 5 is a coreceptor for Alzheimer aβ oligomer bound to cellular prion protein. Neuron 2013;79:887–902.
[46] Hayashi Y, Majewska AK. Dendritic spine geometry: functional implication and regulation. Neuron 2005;46:529–32.
[47] Perez-Cruz C, Nolte MW, van Gaalen MM, Rustay NR, Termont A, Tanghe A, et al. Reduced spine density in specific regions of CA1 pyramidal neurons in two transgenic mouse models of Alzheimer's disease. J Neurosci 2011;31:3926–34.
[48] Androuin A, Potier B, Nägerl UV, Cattaert D, Danglot L, Thierry M, et al. Evidence for altered dendritic spine compartmentalization in Alzheimer's disease and functional effects in a mouse model. Acta Neuropathol 2018;135:839–54.
[49] Boros BD, Greathouse KM, Gentry EG, Curtis KA, Birchall EL, Gearing M, et al. Dendritic spines provide cognitive resilience against Alzheimer's disease. Ann Neurol 2017;82:602–14.
[50] Huijbers W, Mormino EC, Schultz AP, Wigman S, Ward AM, Larvie M, et al. Amyloid-β deposition in mild cognitive impairment is associated with increased hippocampal activity, atrophy and clinical progression. Brain 2015;138:1023–35.
[51] Wang Y, Fu AKY, Ip NY. Instructive roles of astrocytes in hippocampal synaptic plasticity: neuronal activity-dependent regulatory mechanisms. FEBS J 2022;289:2202–18.
[52] Covelo A, Eraso-Pichot A, Fernández-Moncada I, Serrat R, Marsicano G. CB1R-dependent regulation of astrocyte physiology and astrocyte-neuron interactions. Neuropharmacology 2021;195:108678.
[53] Russo EB. Taming THC: potential cannabis synergy and phytocannabinoid-terpenoid entourage effects. Br J Pharmacol 2011;163:1344–64.
[54] Coles M, Steiner-Lim GZ, Karl T. Therapeutic properties of multi-cannabinoid treatment strategies for Alzheimer's disease. Front Neurosci 2022;16:962922.